Paleoceanography and Paleoclimatology

AGU ADVANCING EARTH AND SPACE SCIENCE

RESEARCH ARTICLE
10.1029/2021PA004313

The Late Miocene-Early Pliocene Biogenic Bloom in the Eastern Equatorial Pacific: New Insights From Integrated Ocean Drilling Program Site U1335

Daniele Reghellin[1], Helen K. Coxall[2], Gerald R. Dickens[3], Simone Galeotti[1], and Jan Backman[2]

[1]Department of Pure and Applied Sciences (DiSPeA), University of Urbino Carlo Bo, Urbino, Italy, [2]Department of Geological Sciences, Stockholm University, Stockholm, Sweden, [3]Department of Geology, Trinity College, Dublin, Ireland

Key Points:

- Higher bulk carbonate $\delta^{18}O$ between ca. 5 and 7 Ma suggests cooler SSTs at Site U1335 compared to other off-Equator sites further east
- During the BB the equatorial upwelling band was less parallel to the Equator compared to present day
- During the BB the equatorial upwelling was more intense compared to present day

Supporting Information:

Supporting Information may be found in the online version of this article.

Correspondence to:

D. Reghellin,
daniele.reghellin@uniurb.it

Citation:

Reghellin, D., Coxall, H. K., Dickens, G. R., Galeotti, S., & Backman, J. (2022). The late Miocene-early Pliocene biogenic bloom in the eastern equatorial Pacific: New insights from Integrated Ocean Drilling Program Site U1335. *Paleoceanography and Paleoclimatology*, *37*, e2021PA004313. https://doi.org/10.1029/2021PA004313

Received 21 MAY 2021
Accepted 2 FEB 2022

Abstract The late Miocene-early Pliocene "biogenic bloom" (BB) manifests as greatly enhanced biogenic sedimentation in sites along the Equator that has been linked to cooler sea surface temperature (SST) in the eastern equatorial Pacific (EEP). However, the full extent and geometry of the BB in the EEP is less known. To improve on this, we have generated new carbonate content ($CaCO_3$%) and bulk carbonate stable isotope ($\delta^{13}C$ and $\delta^{18}O$) records spanning the last 7 Ma at IODP Site U1335, located ca. 5° north of the Equator and to the west of the EEP. Site U1335 $\delta^{13}C$ and $\delta^{18}O$ records display high-frequency variations coupled to changes in sediment composition and physical properties comparable to patterns seen at on-Equator sites further east. During the late Miocene and the early Pliocene bulk $\delta^{18}O$ is higher at Site U1335 compared to two off-Equator sites further east, suggesting cooler SSTs generated by stronger equatorial upwelling reaching northwest of the modern core-equatorial upwelling belt. Enhanced upwelling at Site U1335 is supported by relatively higher sedimentation rates prior to 4.6 Ma, symptomatic of higher biological production during the BB. These observations suggest that during the BB the equatorial upwelling circulation was more focused and less parallel to the Equator compared to present day.

1. Introduction

The paleoceanographic "biogenic bloom (BB)" term refers to a widespread increase in marine biogenic primary production, expressed as increased sedimentation rates of biogenic components ($CaCO_3$, SiO_2, P, Ba) in deep-sea sediments deposited during the late Miocene-early Pliocene (ca. 8.0-4.6 Ma) in upwelling areas of the Indian, Pacific, and Atlantic oceans (Anderson & Steinmetz, 1981; Dickens & Owen, 1999; Farrell et al., 1995; Grant & Dickens, 2002; Lyle et al., 2019; Peterson & Backman, 1990; Zhang et al., 2017). At low to mid latitudes, nutrient supply typically limits surface primary productivity (and resulting biogenic accumulation), leading many workers to explain the BB by enhanced nutrient delivery to the photic zone. A root problem has been (Dickens & Owen, 1999): do observations reflect greater upwelling at certain locations (and hence redistribution of nutrients from the subsurface ocean) or higher overall nutrient concentrations in the ocean (and hence excess delivery from riverine and other sources)? A series of studies using bulk and foraminiferal calcite $\delta^{13}C$ and $\delta^{18}O$ as paleoceanographic tracers have argued for intensified wind-driven upwelling driving the enhanced primary productivity along the Pacific Equator during the BB (Pisias & Prell, 1985; Pisias et al., 1995; Reghellin et al., 2015, 2020; Shackleton & Hall, 1995). The remarkable correlation of bulk stable isotope over time across a broad oceanographic region in the eastern equatorial Pacific (EEP), i.e., broader than the inferred zone of wind focused upwelling, however, hint at a rather complex system, likely involving several factors combining to generate the observed geochemical patterns (Reghellin et al., 2020). To gain a better chance of understanding the mechanistic drivers of this inferred strengthened upwelling greater spatial coverage of paleoceanographic records is needed. Focusing on that goal, this study adds new perspectives from an IODP cored at 5° north of the Equator and to the west of the EEP, allowing us to further constrain the extent of the upwelling signals and their evolution through the late Miocene to early Pliocene.

1.1. Eastern Equatorial Pacific Paleoceanography Through the Neogene: Perspectives From Bulk Carbon and Oxygen Stable Isotopes

The EEP is defined as the ocean area between 15°N and 15°S latitude, and between 150°W longitude and the coasts of Central and South America (Figure 1). It is a primary source of CO_2 to the atmosphere (Takahashi

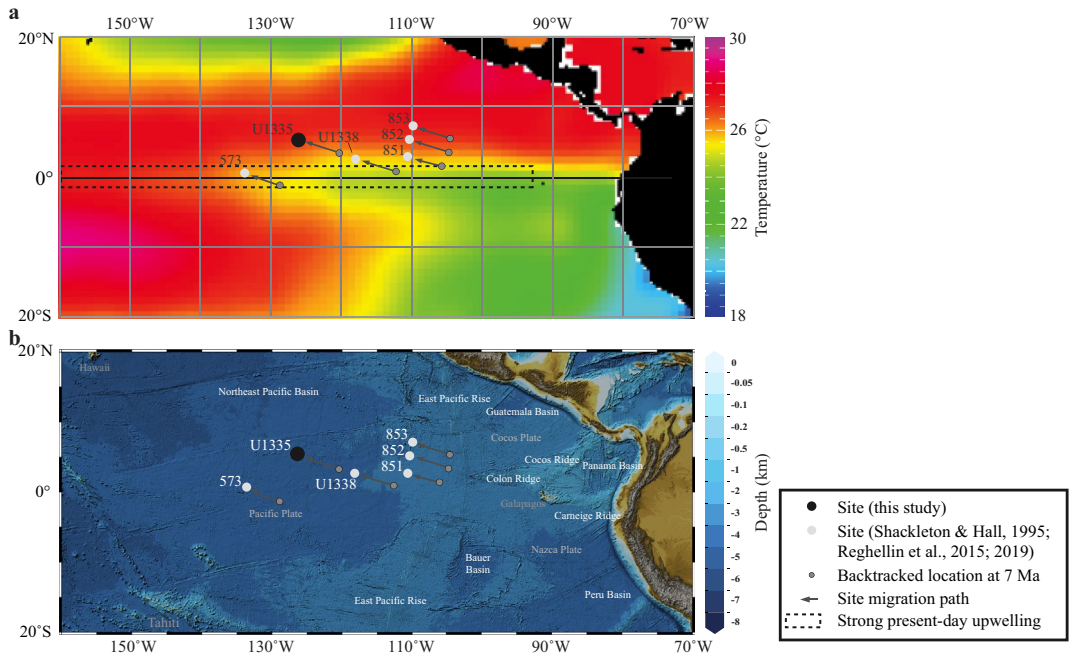

Figure 1. Location of the cored sediment sequences considered in this study and their oceanographic and bathymetric settings in the eastern equatorial Pacific (EEP). (a) Modern mean annual sea surface temperature (SST) and (b) bathymetry. The temperature map is modified from Reghellin et al. (2020). Bathymetric data and map are from GEBCO Compilation Group (2019). Backtracked sites location at 7 Ma and site migration paths are from Weinreich and Theyer (1985) (Site 573), Pisias et al. (1995) (Sites 851, 852, and 853), and Pälike et al. (2010) (Sites U1335 and U1338). The dashed black box represents the area of modern strong wind-driven equatorial upwelling, located at about ±2.5° latitude of the Equator and west of the Galapagos Islands (Fiedler & Lavin, 2017).

et al., 2009) and an important area of ocean-atmosphere heat exchange (Kosaka & Xie, 2013; Linsley et al., 2015), as a consequence of the wind-driven equatorial upwelling that brings cold, CO_2, and nutrient-rich subsurface waters to the surface (Fiedler & Lavín, 2017; Pennington et al., 2006). Understanding its evolution through the Neogene is thus intricately linked to and important for understanding how Earth's climate and ocean subsystems operate under warmer and cooler than modern conditions. In the EEP, the BB is generally linked to (a) cooler sea-surface temperatures (SSTs) along the Equator, (b) expanded meridional (north-south) sea surface temperature (SST) gradients, and (c) higher rates of surface ocean biological productivity (Farrell et al., 1995; Lyle & Baldauf, 2015; Lyle et al., 2019; Pisias et al., 1995; Reghellin et al., 2015; Rousselle et al., 2013; Seki et al., 2012; Shackleton & Hall, 1995; Zhang et al., 2017).

Central to the hypotheses and methodology advocated, here, is the study of Shackleton and Hall (1995), who analyzed the carbon and oxygen stable isotope composition, $\delta^{13}C$ and $\delta^{18}O$ respectively, of bulk carbonate deposited at Ocean Drilling Program (ODP) Leg 138 sites (Pisias et al., 1995) over the last 10 Ma (Figure 1). Their $\delta^{13}C$ records display high amplitude variation over short depth/time intervals that are correlative across sites, both "on" and "off" the Equator (Shackleton & Hall, 1995; Figure 2). The $\delta^{18}O$ records also show high amplitude variation correlative across sites but with two key differences for on-Equator versus off-Equator sites. First, sediment bulk $\delta^{18}O$ values at on-Equator sites were generally higher than those from at off-Equator sites for the entire 0–10 Myr period. Second, between about 8 and 4 Ma, the $\delta^{18}O$ gradient between on-Equator and off-Equator sites is especially large, with on-Equator sites having ca. 1‰ higher $\delta^{18}O$ values. Shackleton and Hall (1995) attributed the expanded $\delta^{18}O$ gradients to larger SST gradients between on-Equator and off-Equator sites, with lower (cooler) SST along the Equator and higher (warmer) SST off the Equator. The expanded SST gradient was explained by an intensified wind-driven circulation during the late Miocene, driving a stronger and more Equator-focused equatorial upwelling (Pisias & Prell, 1985; Pisias et al., 1995; Shackleton & Hall, 1995). This idea is supported by the large increase in biogenic sedimentation at on-Equator sites and, to a lesser extent at off-Equator sites, interpreted as reflecting an expanded high-productivity zone (Figure 2; Lyle et al., 1995; Pisias & Prell, 1985;

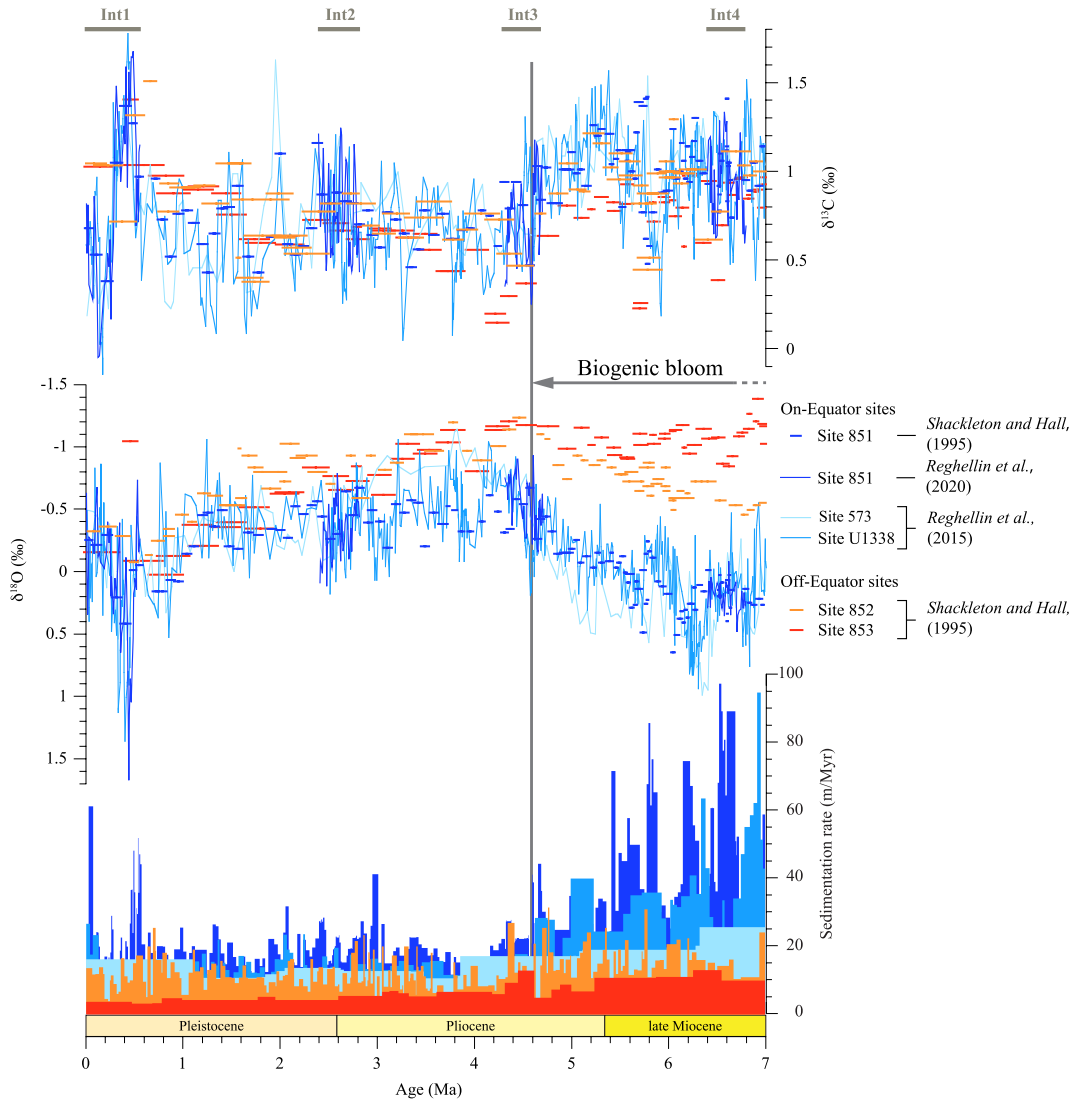

Figure 2. Comparison of relevant published bulk carbonate $\delta^{13}C$ and $\delta^{18}O$ and sedimentation rate records from the eastern equatorial Pacific (EEP) for the last 7 Ma. This includes data at on-Equator Sites 573 (Reghellin et al., 2015), 851 (Reghellin et al., 2020; Shackleton & Hall, 1995), and U1338 (Reghellin et al., 2015) and data at off-Equator Sites 852 and 853 (Shackleton & Hall, 1995). The Shackleton and Hall (1995) data are displayed as bars because samples represent integrated values over core sections, typically 1.5-m length. The vertical gray line represents the end of the BB as suggested by geochemical records at sites examined in this study. Ages for data at Sites 851 come from Reghellin et al. (2020). Ages for data at Sites 573 and U1338 come from Reghellin et al. (2015). Ages for data at Sites 852 and 853 come from Shackleton et al. (1995). Gray bars represent intervals with bulk $\delta^{13}C$ and $\delta^{18}O$ data at Site 851 (Reghellin et al., 2020). Note the coherency of $\delta^{13}C$ records over the last 7 Ma and the ca. 1‰ $\delta^{18}O$ offset between on-Equator and off-Equator Sites during the late Miocene-early Pliocene (ca. 4–8 Ma).

Pisias et al., 1995; Shackleton & Hall, 1995). These observations and interpretations are consistent with BB conditions in the EEP.

However, other sets of proxy data have resulted in very different interpretations of late Miocene-early Pliocene conditions in the EEP resulting in considerable community debate (Table 1). The key alternative idea is that under the ca. 2–3°C warmer-than-modern global conditions of the early Pliocene (ca. 5.3-3.5 Ma), the EEP was characterized by higher SSTs and weaker equatorial upwelling (Ford et al., 2015; Ravelo, 2010; Wara et al., 2005). This scenario is compared to a "permanent El Niño" state, also known as "El Padre" (Ford et al., 2015), where low meridional and weak zonal SST gradients, similar to the conditions of a modern El Niño event, are sustained over much longer time intervals. This interpretation is based on analyses of $\delta^{13}C$, $\delta^{18}O$, and Mg/Ca ratios measured

Table 1
Overview of the Main Published Studies Discussing Eastern Equatorial Pacific (EEP) Paleoceanography During the Late Miocene and the Early Pliocene With the Main Proxies Used to Reconstruct SST and the Scenario Proposed

Reference	Proxy type	Paleoceanographic scenario
Shackleton and Hall (1995)	Bulk carbonate $\delta^{13}C$ and $\delta^{18}O$	Intense upwelling/cool SST
Wara et al. (2005)	Foraminifera $\delta^{13}C$ and $\delta^{18}O$, Mg/Ca	Weak upwelling/warm SST
Lawrence et al. (2006)	Foraminifera Mg/Ca, $U^{k'}37$	Weak upwelling/warm SST
Ravelo et al. (2006)	Foraminifera Mg/Ca, $U^{k'}37$	Weak upwelling/warm SST
Dekens et al. (2007)	Foraminifera Mg/Ca, $U^{k'}37$	Intense upwelling/warm SST
Nathan and Leckie (2009)	Foraminifera $\delta^{13}C$ and $\delta^{18}O$	Fluctuations between intense and weak upwelling
Ravelo (2010)	Foraminifera Mg/Ca, $U^{k'}37$	Weak upwelling/warm SST
Steph et al. (2010)	Foraminifera $\delta^{13}C$ and $\delta^{18}O$, Mg/Ca, $U^{k'}37$	Weak upwelling/warm SST
Ford et al. (2012)	Foraminifera $\delta^{13}C$ and $\delta^{18}O$, Mg/Ca	Weak upwelling, deep thermocline/warm SST
LaRiviere et al. (2012)	Foraminifera $\delta^{18}O$, Mg/Ca, $U^{k'}37$	Weak upwelling/warm SST
Seki et al. (2012)	TEX86, $U^{k'}37$	Intense upwelling/cool SST
Rousselle et al. (2013)	$U^{k'}37$, fine fraction $\delta^{18}O$	Intense upwelling/cool SST
Beltran et al. (2014)	$U^{k'}37$	Weak upwelling/warm SST
Ford et al. (2015)	Foraminifera Mg/Ca	Weak upwelling, deep thermocline/warm SST
Reghellin et al. (2015)	Bulk/fine carbonate $\delta^{13}C$ and $\delta^{18}O$	Intense upwelling/cool SST
Zhang et al. (2014)	TEX86, $U^{k'}37$	Intense upwelling/cool SST
Zhang et al. (2017)	TEX86, $U^{k'}37$	Intense upwelling/warmer water column
Drury et al. (2018)	Foraminifera $\delta^{13}C$ and $\delta^{18}O$, Mg/Ca	Weak upwelling; intense upwelling at 6.5-5.7 Ma
Liu et al. (2019)	$U^{k'}37$	Warm SST

on planktonic foraminifera tests, and alkenone ratios ($U^{k'}_{37}$; Beltran et al., 2014; Ford et al., 2012, 2015; Lariviere et al., 2012; Lawrence et al., 2006; Ravelo, 2010; Ravelo et al., 2006; Seki et al., 2012; Steph et al., 2010; Wara et al., 2005). Permanent El-Niño-like conditions implying strong thermal stratification is opposite to the stronger upward mixing and surface fertilization scenario invoked to explain the high export production of the BB, and the two interpretations seem incompatible (Lea, 2014). Further studies proposed a decoupling between ocean temperature and upwelling intensity to explain the divergent scenarios derived from different proxies (Lyle & Baldauf, 2015; Zhang et al., 2017). According to these studies the increased upwelling is compatible with higher water temperatures because of: (a) the warmer-than-modern water column and a shallower thermocline during the late Miocene (Zhang et al., 2017) or (b) warmer-than-modern extratropical waters that fueled the EEP upwelling system during BB time (Liu et al., 2019).

However, there remain uncertainties in proxy temperature data and difficulties in calculating temperature gradients using heterogeneous proxy datasets. Moreover, these divergent scenarios are partly resulting from four basic challenges that hamper paleoceanographic investigations in the EEP. First, the region is highly dynamic with steep zonal (east-west) and meridional gradients in many ocean properties, such as SST, biogenic particle production, and sedimentation (Barber & Chávez, 1986; Kessler, 2006; Trenberth & Caron, 2000), and CO_2 air-sea fluxes (Kozyr, 2008; Takahashi et al., 2002, 2009). These properties can change abruptly over quasi-periodic semidecadal cycles because of changes in ocean and atmosphere circulation (Holbrook et al., 2012). A second problem relates to bathymetry, with depths roughly increasing westward (Figure 1). Most of the region lies below 4,000 m water depth and hence is below the lysocline, where the rate of calcite dissolution increases rapidly (Farrell & Prell, 1989; Farrell et al., 1995; Lyle, 2003; Lyle et al., 2019). This implies that biogenic carbonate tests, especially those of planktonic foraminifera (importance proxy signal carriers), may be biased by dissolution and recrystallization (Lyle et al., 2019; Pälike et al., 2012; van Andel et al., 1975). Third, tectonic changes during the late Miocene-early Pliocene include closure of the Panama seaway, restriction of the Pacific-Indian Ocean Indonesian throughflow and uplift of the Andes Mountains, each of which have potential to impact global oceanography (Auer et al., 2019; Brierley & Fedorov, 2016; Garzione et al., 2008; O'Dea et al., 2016; Schneider, 1998;

Steinthorsdottir et al., 2021). Fourth, divergent paleoceanographic interpretations may arise due to complexities in the understanding of the environmental signal captured by the various proxies in such a dynamic ocean area (Lea, 2014). For example, paleoceanographic interpretations of bulk carbonate $\delta^{13}C$ and $\delta^{18}O$ are complicated because bulk carbonate consists of multiple microfossil and nannofossil contributors, each with potentially different isotopic fractionations due to their characteristic ecologies (Reghellin et al., 2015, 2020).

To better understand bulk sediment $\delta^{13}C$ and $\delta^{18}O$ as an EEP proxy, Reghellin et al. (2015, 2020) generated new bulk $\delta^{13}C$ and $\delta^{18}O$ records from on-Equator Sites 573 and U1338, and on bulk and multiple isolated sediment fractions from on-Equator Site 851 (Figures 1 and 2). These studies confirmed Shackleton and Hall's (1995) observations of correlative bulk isotopes records along the Equator in the EEP, and demonstrated that EEP bulk records primarily reflect the stable isotope composition of photosynthesizing coccolithophores, by far the most significant sedimentary contributor (typically >90% of the carbonate fraction) at the examined on-Equator sites. The bulk carbonate $\delta^{13}C$ and $\delta^{18}O$, thus reflect upper mixed layer chemical properties and temperature variability albeit with some modification by "vital effects" (Reghellin et al., 2020).

Data from on-Equator Sites 573, 851, and U1338 (Reghellin et al., 2015, 2020) are consistent with previous data showing higher bulk $\delta^{18}O$ and increased sedimentation rates during the late Miocene and the early Pliocene (Farrell & Prell, 1989; Pisias et al., 1995; Shackleton & Hall, 1995), supporting the idea of late Miocene-early Pliocene BB conditions along the Equator in the EEP. However, the spatial extent of BB conditions in the EEP is still not fully clear. This is because available bulk isotopes data are (a) mainly from on-Equator sites (Reghellin et al., 2015, 2020; Shackleton & Hall, 1995) and (b) only from off-Equator Sites 852 and 853, limited to the eastern EEP, whereas coverage to the northwest is needed to better document the regional picture (Figure 1). Moreover, Shackleton and Hall (1995) analyzed sediments scraped from the surface of each 1.5-m long core section, thus, each of their bulk $\delta^{13}C$ and $\delta^{18}O$ analysis represents an average over the 1.5-m long intervals (long bar symbols in Figure 2), which is insufficient for resolving important finer scale variability of the EEP system.

Here, we present new carbonate content ($CaCO_3$%) and bulk carbonate $\delta^{13}C$ and $\delta^{18}O$ records from Integrated Ocean Drilling Program (IODP) Site U1335 (Figure 1) that span the last 7 Myr. Site U1335 lies at about 5°N latitude and provides an "off-Equator" perspective to the west of previous off-Equator records and will be useful to either support, or reconsider, previous ideas of intensified wind-driven upwelling in the EEP during the late Miocene and the early Pliocene. This site has remained >2.5° north of the Equator since 7 Ma (Pälike et al., 2010), suggesting that changes in sediment properties and composition likely reflect changes related to upwelling conditions rather than site migration on the northwestward moving Pacific Plate. Site U1335 lies at a greater water depth (>4.3 km) than other EEP sites having bulk sediment stable isotopes, providing an opportunity to explore the impact of sublysocline carbonate dissolution on bulk sediment geochemical signals. The new bulk isotope data from Site U1335 were generated to help answer the following questions:

1. Are high-frequency variations in bulk carbonate isotope records also present at Site U1335?
2. Is bulk carbonate $\delta^{18}O$ at Site U1335 similar to other off-Equator bulk $\delta^{18}O$ records, showing ca. 1‰ lower values than on-Equator sites during the BB?
3. During the BB, how does sedimentation rates at Site U1335 compare to those at other on-Equator and off-Equator sites?
4. Are these new bulk carbonate isotope data consistent with a more intense and Equator-parallel wind-driven ocean circulation during the BB, compared to the present?

2. Materials and Methods

2.1. IODP Site U1335

Site U1335 is located above ca. 26 Ma old crust at 5°18.7′N latitude, 126°17.0′W longitude, at a water depth of 4327.5 m below sea level (Pälike et al., 2010). Two holes (A and B) were APC-cored to 341 and 378 m below seafloor (mbsf), respectively. The sediments consist of late Miocene to Pleistocene multicolored calcareous nannofossil, foraminifera, and diatom oozes and are characterized by decimeter-scale to centimeter-scale alternations in sediment color, and physical properties, representing changes in $CaCO_3$% at orbital time scales (Lyle et al., 2019; Figure 3). Site U1335 moved to the northwest for about 700 km over the last 7 Myr (Figure 1), but

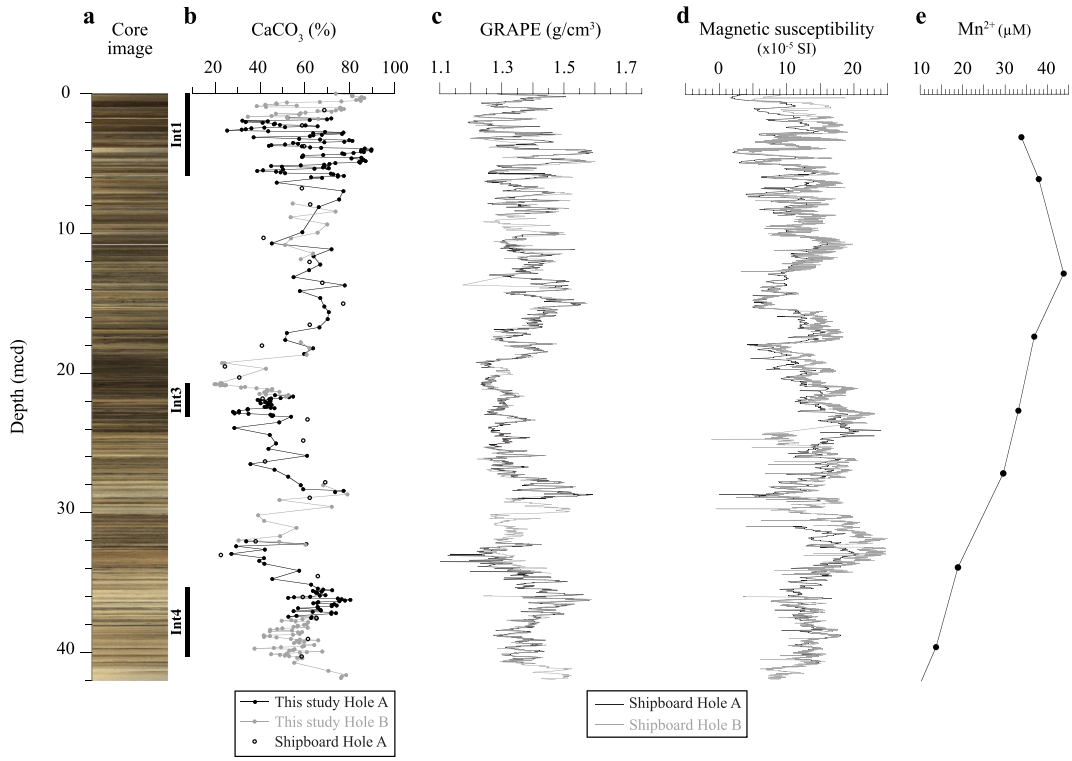

Figure 3. Site U1335 downcore physical and chemical properties. (a) Composite core image, (b) carbonate content ($CaCO_3$%), (c) Gamma Ray Attenuation Porosity Evaluator (GRAPE) measurements (approximating wet bulk density), (d) magnetic susceptibility (MS), and (e) dissolved manganese in pore water at Site U1335. Black bars represent the three time intervals with records at higher resolution. $CaCO_3$% data come from shipboard measurements (Pälike et al., 2010) and this study. GRAPE, MS, and dissolved manganese (Mn^{2+}) data come from shipboard measurements (Pälike et al., 2010).

remained outside the region of strong present day wind-driven equatorial upwelling (±2.5° of latitude; Fiedler & Lavín, 2017; Pälike et al., 2010).

2.2. Sampling Strategy

A total of 335 samples were selected from Site U1335, following a spliced composite section spanning 0–42 m composite depth (mcd; Table S1 in Supporting Information S1). Each sample has a volume of 5 cc and was collected spanning 1 cm of vertical thickness. Of the 335 samples, 259 were selected to produce records with higher spatial and temporal resolution, across three depth/time intervals (Table S1 in Supporting Information S1). These three intervals where selected to cover similar depth/age ranges of intervals with published $CaCO_3$%, bulk carbonate and foraminifera stable isotope data at Site 851 (Figure 2; Reghellin et al., 2020). For consistency, we kept the same labeling for intervals with similar age ranges: 0–0.9 Ma—Interval 1 (*Int1*); 4.0–4.4 Ma—Interval 3 (*Int3*); 6.2–6.8 Ma—Interval 4 (*Int4*), which includes the acme of the BB.

Sample spacing within the three intervals is 5.3 cm and 8.1 kyr on average; sedimentation rates vary significantly in the three intervals (Table S1 in Supporting Information S1). The remaining 76 samples were selected to fill the gaps between the three intervals over the last 7 Ma with records at lower spatial and temporal resolution (on average 34.1 cm, 49.9 kyr).

2.3. Carbonate Analyses

The bulk sediment $CaCO_3$% was measured using the coulometry method (Mörth & Backman, 2011). For each sample, 30–35 mg of powdered sediment was put into a dry and clean Teflon cup. $CaCO_3$% was determined from the reaction of sediment with 2 mL of 2 M hydrochloric acid. The acid was injected into the coulometer sample tube, so it completely drowned the sediment sample. The measurement precision is ±0.8%.

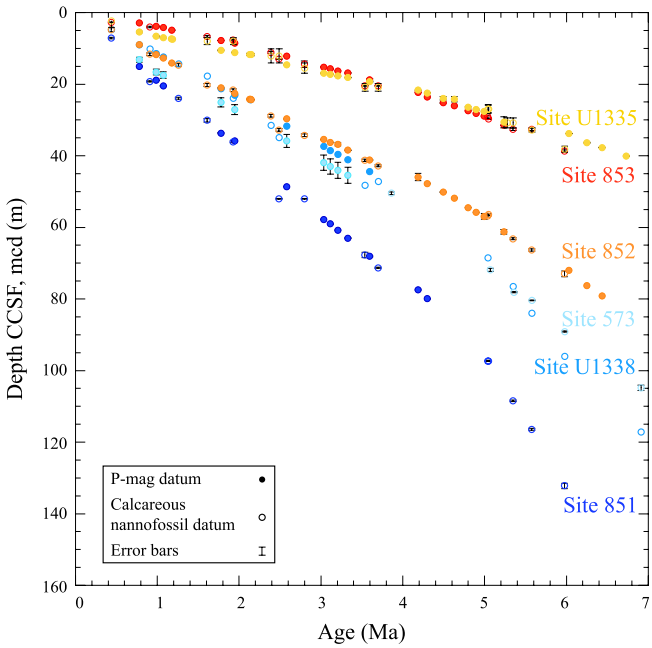

Figure 4. Sediment age-depth relationships constrained by biostratigraphic and magnetostratigraphic markers for Sites 573, 851, 852, 853, U1335, and U1338. These includes geomagnetic reversal boundaries and first and last occurrence of calcareous nannofossils species (Backman et al., 2013; Pälike et al., 2010; Raffi & Flores, 1995; Shipboard Scientific Party, 1992; Weinreich & Theyer, 1985). All age markers shown in the figure have been placed onto a common time scale (Lourens et al., 2004). All sites display increased sedimentation rates in the late Miocene and early Pliocene, which reflects greater biogenic sedimentation during the BB across the eastern equatorial Pacific (EEP).

2.4. Stable Isotope Analyses

Stable isotope analyses were performed at the Department of Geological Sciences, Stockholm University, using a Finnigan Mat 252 IRMS coupled with a Finnigan Gasbench II device.

Sample aliquots corresponding to 0.25 mg of pure $CaCO_3$ were added to a septum-seal glass vial, flushed with gaseous helium and reacted with excess of 100% phosphoric acid at room temperature for 18 hr. Two international (IAEA-CO-1 and NBS19) and two in-house ($CaCO_3$ and Merck Carm-1) standards were analyzed with the samples to estimate the analytical precision of these measurements (Révész & Landwehr, 2002), which is ±0.07‰ for $\delta^{13}C$ and ±0.15‰ for $\delta^{18}O$. Results are expressed in per mil (‰) and reported relative to Vienna Pee Dee Belemnite (PDB).

2.5. Age Model and Sedimentation Rates

To align the new records at Site U1335 with published data across the EEP (Figure 4), we calculate age of sediment samples at Site U1335 and at Site U1338 (Reghellin et al., 2015) using the astronomically tuned age model of Lyle et al. (2019). We have assumed linear sedimentation rate (LSR) between two successive age markers and are aware that the assumption of LSR between age tie points leads to inaccuracies of age estimations. However, the age estimation errors should be <50 kyr for any sample.

3. Results

3.1. Carbonate Content

The $CaCO_3$% signal displays large amplitude variations over short depth/time intervals as well as long-term trends over the studied sedimentary section (Table S1 in Supporting Information S1). $CaCO_3$% ranges between 19.8% and 89.6%, and averages 57.6%. Changes in $CaCO_3$% correspond to changes in sediment color and physical properties (Figure 3). Intervals with low $CaCO_3$%, are generally darker in color, have lower Gamma Ray Attenuation Porosity Evaluator (GRAPE) values (that approximate sediment wet bulk density, WBD), and higher magnetic susceptibility (MS). Intervals with high $CaCO_3$%, are generally lighter in color, have higher GRAPE values, and lower MS values. In addition, $CaCO_3$% shows a positive second-order relationship with WBD (Figure S1 in Supporting Information S1). Carbonate content at Site U1335 generally decreases from present day to about 4 Ma (Figure 5). Before 4 Ma, $CaCO_3$% generally increases with increasing depth and age, although low $CaCO_3$% values (<40%) are registered at about 5.8 and 6.8 Ma. Across the entire *Int1* the $CaCO_3$% exhibits the largest amplitude variations of the whole record, with variations greater than 40% over ca. 0.5 m or 75 kyr (Figures 3 and 5).

3.2. Carbon Isotope Composition of Bulk Carbonate

The bulk carbonate $\delta^{13}C$ record exhibits both long-term trends and short-term variations (Figure 5), ranging between 0.17‰ and 1.79‰ and averages 0.89 ± 0.28‰ (1σ standard deviation used throughout the text; Table S1 in Supporting Information S1). There is a general $\delta^{13}C$ decrease from 0 to 2 Ma, although lowest (0.39 ± 0.15‰ on average) and highest (1.38 ± 0.28‰ on average) values over the last 7 Ma occur at ca. 0.1 and 0.5 Ma, respectively (Figure 5). Between about 2 and 4 Ma bulk $\delta^{13}C$ slightly increases by ca. 0.15‰ on average. Before 4 Ma, the bulk $\delta^{13}C$ generally decreases reaching values lower than 0.5‰ in the late Miocene at about 6.4 and 6.8 Ma.

3.3. Oxygen Isotope Composition of Bulk Carbonate

The bulk carbonate $\delta^{18}O$ record exhibits both long-term and short-term changes over the last 7 Ma (Figure 5), with values ranging between −1.12‰ and 1.02‰ and averages −0.28 ± 0.31‰ (Table S1 in Supporting

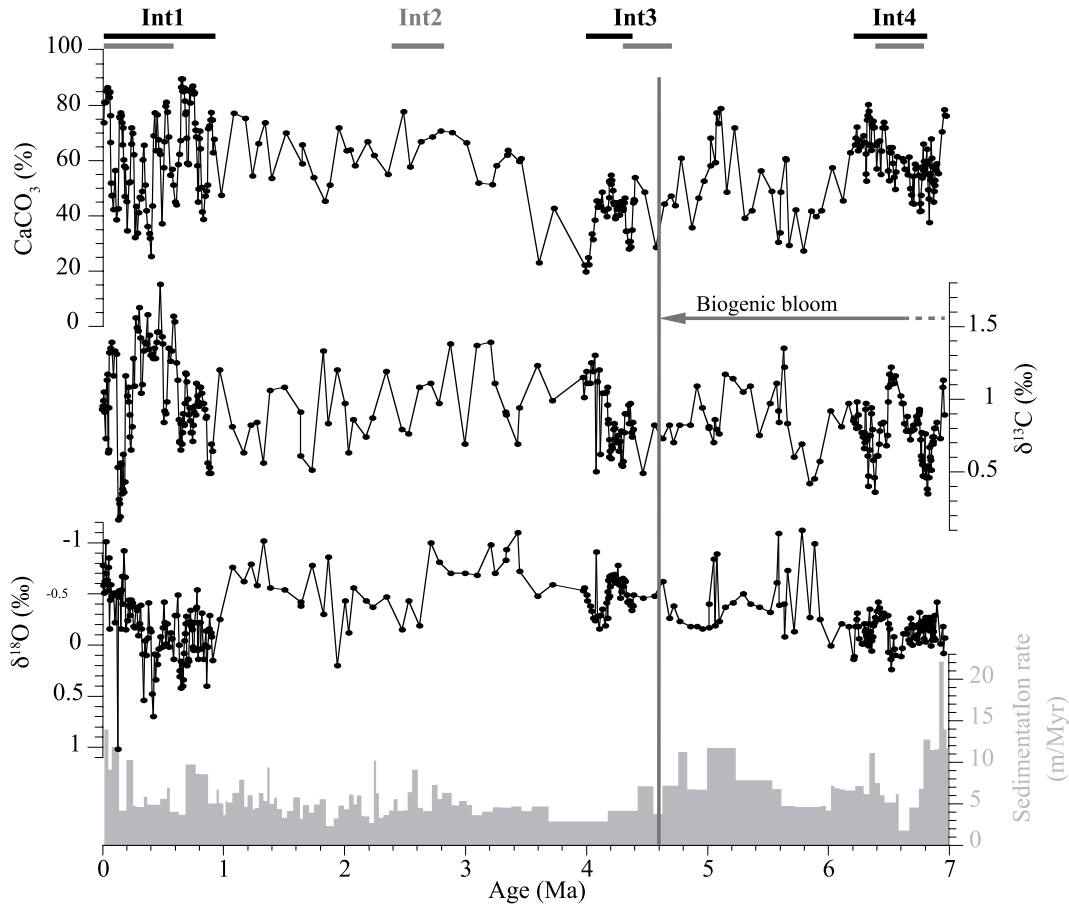

Figure 5. $CaCO_3$%, bulk carbonate $\delta^{13}C$ and $\delta^{18}O$, and sedimentation rate records at ODP Site U1335. Black bars represent the three time intervals with records at higher resolution, whereas gray bars represent the intervals analyzed by Reghellin et al. (2020). The vertical gray line represents the end of the BB as suggested by geochemical records at sites examined in this study. Ages for samples were determined using the age model of Lyle et al. (2019).

Information S1). Bulk $\delta^{18}O$ increases from present day to about 0.4 Ma (Figure 5), then generally decreases until about 3.4 Ma. Before 3.4 Ma bulk, $\delta^{18}O$ reach values of ca. −0.1‰ on average in the late Miocene. Despite the increasing trend, bulk $\delta^{18}O$ shows significantly low values (<−0.8‰) in five samples, two centered at about 5.1 Ma, and the remaining three centered at about 5.8 Ma (Figure 5; Table S1 in Supporting Information S1).

4. Discussion

4.1. Relationship Between Sediment Composition and WBD at Site U1335

The new $CaCO_3$% record at Site U1335 is consistent both with shipboard data (Figure 3; Pälike et al., 2010) and data derived from X-ray Fluorescence (XRF; Lyle et al., 2019; Shackford et al., 2014). The $CaCO_3$% shows large amplitude changes (up to 38%) over centimeter-scale to decimeter-scale depth intervals, which relate to changes in sediment color, GRAPE, and MS (Figure 3). Sediments at Site U1335 show a positive second-order relationship between $CaCO_3$% and WBD (Figure S1 in Supporting Information S1), consistent with previous observations from Site U1338 (Reghellin et al., 2013), and indicates a wide range in WBD for a given $CaCO_3$% value. This implies that sediment at Site U1335 consists of three main components, each with different grain density and porosity: (a) fine biogenic carbonate particles, mostly calcareous nannofossils, (b) coarse biogenic carbonate particles, mostly planktonic foraminifera, and (c) biogenic silica, mostly diatoms, and Radiolaria.

4.2. Sediment Color

In the EEP, darker sediments typically represent intervals richer in biogenic silica whereas lighter sediments represent intervals richer in biogenic carbonate (Pälike et al., 2010). Sediment color becomes lighter with increasing burial depth over the studied interval at Site U1335 (Figure 3). However, the lighter sediment color below 24 mcd compared to above 24 mcd is not directly linked to higher $CaCO_3$%: carbonate content averages 57.5% between 0 and 24 mcd (darker) and 57.9% between 24 and 42 mcd (lighter; Table S1 in Supporting Information S1). A possible explanation is lower concentrations of dark-colored manganese-rich minerals (Pälike et al., 2010), as indicated by the decreasing downcore porewater Mn^{2+} profile (Figure 3). Shipboard measurements of Mn^{2+} concentration in interstitial water show values >33 μM in the upper ca. 23 mcd of sediment with a high peak of 43.8 μM at 13 mcd. Below 13 mcd, the Mn^{2+} concentration decreases, reaching values of <15 μM at 39 m. Metallic oxides in interstitial water can precipitate into authigenic carbonates, e.g., rhodochrosite ($MnCO_3$), which are dark in color, or coat existing carbonate particles (Hesse & Schacht, 2011). The decreasing Mn^{2+} concentration indicates that microbial reactions are consuming manganese oxides below 13 mcd. This process removes manganese authigenic carbonates, and may have resulted in the observed lighter sediment color with depth (Figure 3), despite the absence of an average increase of $CaCO_3$% in the 0–42-mcd interval.

4.3. Carbonate Deposition and Preservation at Site U1335

In the stratigraphic interval corresponding to the last 7 Myr, the average $CaCO_3$% at Site U1335 is 58%. This value is clearly lower than observed at on-Equator Sites U1338 (67%), 851 (78%), and 573 (79%; Reghellin et al., 2015, 2020), as well as off-Equator Sites 852 (76%) and 853 (71%; Farrell et al., 1995; Figure 6). Three factors may explain the >9% lower average $CaCO_3$% at Site U1335: (a) greater carbonate dissolution at greater water depth, (b) lower production of biogenic carbonate particles, and (c) dilution by biogenic silica particles and clays.

1. Increased dissolution with depth: Site U1335 is the deepest of the sites examined in this study (Figure 1). Presently, the lysocline depth across the EEP ranges between 3.5 and 4.0 km and was shallower in the late Miocene (Archer, 1991; Berger, 1973; Farrell & Prell, 1989; Farrell et al., 1995; Lyle & Wilson, 2006). Carbonate dissolution thus impacted the $CaCO_3$% at Site U1335 more severely when compared to Sites 851, 852, 853, and U1338, which are several hundreds of meters shallower. We suggest that dissolution was stronger in the upper part of the sedimentary succession at Site U1335 because of the increasing seafloor depth with time
2. Lower production of biogenic carbonate: In the EEP, the production of biogenic $CaCO_3$ is, in general, higher at the Equator where the wind-driven upwelling is strongest and decreases with increasing latitude across the margins of the North Equatorial Current (Fiedler & Lavín, 2017; Honjo et al., 1995; Lyle et al., 2019), which marks the lower branch of the warm and nutrient poor North Pacific Gyre (Honjo et al., 1995). Site U1335 is presently located at about 5°N latitude and, similar to Sites 852 and 853, remained north of 2.5°N latitude over the last 7 Myr. Conversely, on-Equator Sites U1338, 851, and 573 remained within the zone of strong wind-driven upwelling over the same time interval (Figure 1). The lower average value of $CaCO_3$% at Site U1335 might, therefore, reflect both lower biogenic carbonate production and more severe carbonate dissolution when compared to on-Equator sites. Differently, lower carbonate production cannot be invoked to explain the lower values observed in comparison to off-Equator Sites 852–853, greater sublysocline carbonate dissolution at the greater water depth of Site U1335 remaining a plausible mechanism
3. Dilution by biogenic silica and clays: Changes in flux of biosilica and clay particles could potentially act as diluents, lowering the $CaCO_3$% at Site U1335. Comparison between published XRF-derived, normalized median-scaled biosilica content (SiO_2NMS%) record (Lyle et al., 2019) and new $CaCO_3$% record clearly shows that intervals of high $CaCO_3$% correspond to intervals of low SiO_2NMS% and vice versa throughout the last 7 Myr (Figure S2 in Supporting Information S1). These results are consistent with the WBD-$CaCO_3$% relationship (Figure S1 in Supporting Information S1), implying that intervals with higher $CaCO_3$% have lower biosilica content and vice versa. However, given the lower biological production off the Equator over the late Neogene, biosilica presumably dilutes carbonate to a lesser extent at Site U1335 than at on-Equator sites. Clays, mainly eolian material, are a minor sediment component (≤10%) compared to biogenic carbonate and biosilica in late Neogene sediments deposited across the EEP (Farrell et al., 1995; Hovan, 1995; Pälike et al., 2010; Pisias et al., 1995). Thus, clays are not a significant diluent at Site U1335 (Pälike et al., 2010)

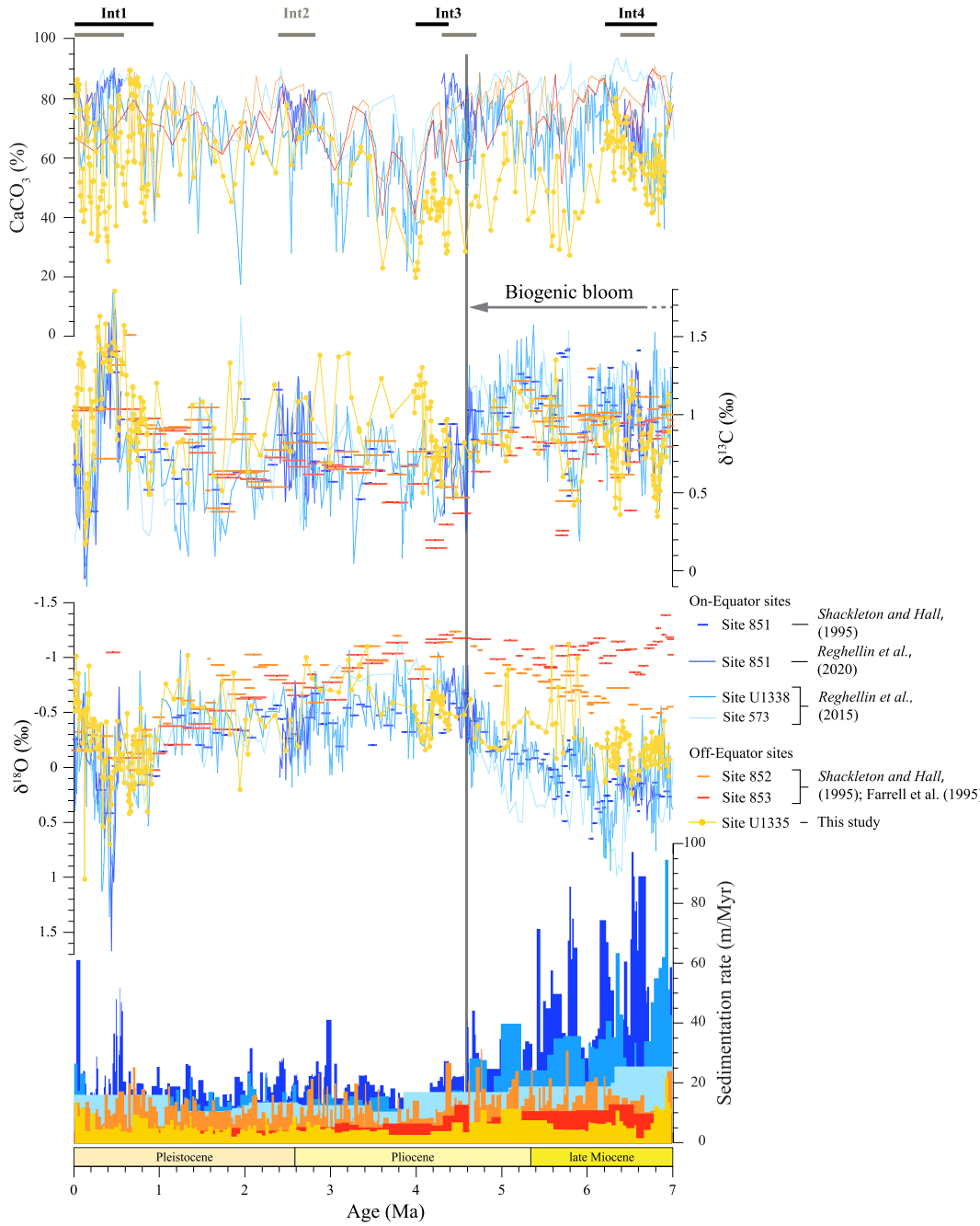

Figure 6. Comparison between relevant published $CaCO_3$%, bulk carbonate $\delta^{13}C$ and $\delta^{18}O$ and sedimentation rate records from the eastern equatorial Pacific (EEP) for the last 7 Ma at Site 851 with new data from Site U1335 (this study). The vertical gray line represents the end of the biogenic bloom (BB; ca. 4.6 Ma) as suggested by geochemical records at sites examined in this study. Ages for samples at Sites U1335 and U1338 were determined using the age model of Lyle et al. (2019). Sample ages for the other sites use the same schemes as for Figure 2. Note that Site U1335 $\delta^{18}O$ displays much similar values compared to on-Equator sites than off-Equator sites, suggesting BB conditions at site location. The low linear sedimentation rate (LSR) even during the BB is due to intense carbonate dissolution at Site U1335.

4.4. Source of Bulk Carbonate $\delta^{13}C$ and $\delta^{18}O$ Signature at Site U1335

Coherent patterns in bulk stable isotope (C, O) variability occur at locations having different sedimentation rates over the last 7 Myr, the most dramatic difference being the much greater LSR at on-Equator sites between 7 and 5 Ma (Figure 6). This implies that stable isotope records do not result from diagenesis in EEP sediments (Hesse &

Schacht, 2011; Reghellin et al., 2020), and therefore represent primary precipitation of calcite at both on-Equator and off-Equator sites.

The dominant carbonate component in sediment deposited within the EEP since the late Miocene are members of the phylomorphogenetic reticulofenestrid calcareous nannofossil lineage (Bolton et al., 2010; Mayer et al., 1985; Pälike et al., 2010; Pisias et al., 1995; Raffi & Flores, 1995). The second most abundant carbonate component are tests of planktonic foraminifera, generally comprising up to 15 wt % at on-Equator Sites U1338, 851, and 573 (Reghellin et al., 2013, 2015, 2020). The proportion of planktic foraminifera tests at Site U1335 is presumably lower than at on-Equator sites, considering the greater sensitivity of planktic foraminifera calcite to sublysocline dissolution (Berger, 1973). Benthic foraminifera are a minor component in deep-sea sediments (ca. <1%; Conan et al., 2002; Hayward et al., 2002). The contribution of foraminifera calcite to bulk $\delta^{13}C$ and $\delta^{18}O$ records at Site U1335 is thus minor, implying that these records primarily reflect the stable isotope composition of reticulofenestrid coccolith calcite, and conditions in the upper 50 m of the water column (Reghellin et al., 2020). Bulk $\delta^{13}C$ and $\delta^{18}O$ at Site U1335 by-and-large hence reflects water chemistry and temperature in the upper mixed layer were these coccolithophorids dwell (Anderson & Steinmetz, 1981, 1983; Hagino et al., 2000; Honjo & Okada, 1974; Steinmetz, 1994).

In the upper 50 m of the water column and within the area where the studied sites are situated, the annual variance of mean ocean water salinity is limited (≤0.5 psu; Locarnini et al., 2019), and it is assumed to have been similar back over past 7 Myr, on late Neogene time scales. Thus, the impact of salinity on bulk $\delta^{18}O$ is negligible (Conroy et al., 2014). Changes in bulk $\delta^{18}O$ can be interpreted as reflecting variations in SST spatially and over time. This is evident when bulk $\delta^{18}O$ measured in surface sediment along the Equator are compared to modern SST (Figure S3 and Table S2 in Supporting Information S1). Hence, from now on bulk $\delta^{18}O$ is considered to track changes in SST, despite this proxy cannot be employed to quantitively reconstruct SST across the EEP.

4.5. Paleoceanographic Interpretation of Bulk $\delta^{13}C$ and $\delta^{18}O$ at Site U1335

4.5.1. Coherent Bulk $\delta^{13}C$ Across the EEP

The new bulk $\delta^{13}C$ record at Site U1335 extends previous observations of covarying bulk $\delta^{13}C$ records along the Equator (Reghellin et al., 2015, 2020; Shackleton & Hall, 1995) to an off-Equator site located 1,800 km west of Leg 138 off-Equator sites (Figures 1 and 6). These results imply similar high-frequency variations in multiple surface water chemistry parameters, including concentration and $\delta^{13}C$ of dissolved inorganic carbon ($\delta^{13}C_{DIC}$), across the EEP throughout the past 7 Myr, despite large ocean conditions variability in the region over interannual scale (Kroopnick, 1985; Reghellin et al., 2015, 2020; Tagliabue & Bopp, 2008). These observations are consistent with variations ≤02.‰ of $\delta^{13}C_{DIC}$ in surface water across the modern EEP (Kroopnick, 1985; Tagliabue & Bopp, 2008), and imply a homogenous $\delta^{13}C_{DIC}$ distribution across the EEP, with differences <0.3‰ at any given time since 7 Ma (above references). Crucially the covarying bulk $\delta^{13}C$ at different sites suggests EEP-wide changes in surface water inorganic carbon chemistry over time since the late Miocene.

4.5.2. The Biogenic Bloom Across the EEP

The new data from Site U1335 represent the first bulk isotope and $CaCO_3$% data from an off-Equator site in the northwestern EEP and help understand how the BB was spatially distributed across the EEP. At Site U1335, bulk $\delta^{18}O$ and LSRs are 0.13‰ and 2%, respectively, higher during the BB compared with post-BB times, reflecting lower SST and enhanced biological production in surface waters generated by enhanced equatorial upwelling (Lyle et al., 2019; Figure 5). Moreover, bulk $\delta^{18}O$ displays higher values compared to other off-Equator sites and lower values compared to on-Equator sites (Figure 6). For example, between 7 and 5 Myr average bulk $\delta^{18}O$ is, at Site U1335, 0.5‰ higher than at off-Equator Site 852 and 0.4‰ lower than at on-Equator Site U1338 (Reghellin et al., 2015; Shackleton & Hall, 1995). The $\delta^{18}O$ offset between Site U1335 and off-Equator sites is unexpected. Considering the meridional bulk $\delta^{18}O$ gradients in published records (Figure 2; Reghellin et al., 2015, 2020; Shackleton & Hall, 1995) and modern meridional SST gradients with isotherms roughly parallel to the Equator (Figure 1; Fiedler & Lavín, 2017), bulk $\delta^{18}O$ at Sites U1335 and 852 might be expected to be similar because the two sites are today located at about the same latitude and presumably were located at similar latitudes over the last 7 Myr (Pälike et al., 2010; Pisias et al., 1995). Instead, the higher bulk $\delta^{18}O$ reflects cooler SST at U1335 compared to Site 852 during the late Miocene and early Pliocene (Figure 7). This implies that, during the BB, the upwelling of cool intermediate water off the Equator was stronger to the west of the EEP, where Site U1335

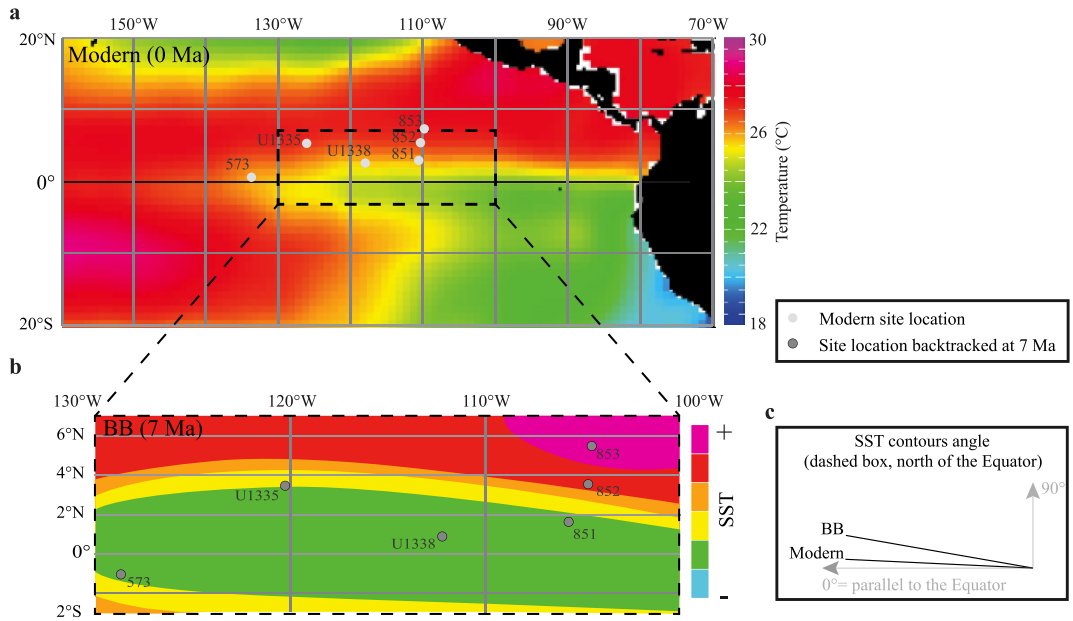

Figure 7. Comparison between the eastern equatorial Pacific (EEP) wind-driven equatorial upwelling system under modern and reconstructed biogenic bloom (BB) conditions. Modern average SST (a), qualitative SST gradients at 7 Ma inferred from bulk stable isotopes, $CaCO_3$% and linear sedimentation rate (LSR) at sites discussed in this study (b) and inclination of SST contours under modern and BB conditions (c). Given the large N-S gradients in surface water properties across the EEP, BB conditions reconstruction is restricted to the area adjacent to the backtracked location at 7 Ma of the sites examined, which roughly correspond to the Ocean area comprised between 3°S and 7°N latitude and between 100°W and 130°W longitude (dashed black box in panel a). The inclination angles of SST contours refer only to the area north of the Equator and within the dashed box. The BB was at its acme at about 7 Ma in the EEP as indicated by the bulk sediment proxies at multiple locations across the EEP. Note that during the BB meridional SST gradients were greater compared to present day as indicated by warmer SST at Sites 852 and 853. However, SST was cooler at Site U1335 compared to modern suggesting that equatorial upwelling circulation was less parallel to the Equator compared to modern, with SST contours moving northwards with increasing longitude.

was located (ca. 120°W longitude), compared to the east, where Site 852 was located (ca. 105°W longitude). This zonal gradient off the Equator seems to reflect an equatorial upwelling area less parallel to the Equator compared to present day, with more tilted isotherm contour patterns (Figure 7). The lower bulk $\delta^{18}O$ at Site U1335 compared to on-Equator sites suggests warmer SST than along the Equator during the BB.

The comparison between bulk $\delta^{18}O$ average values from each site at 7 Ma with those at present potentially can add information on SST gradients and may help understanding of the BB geometry during the BB. At Sites 853 and 852 bulk $\delta^{18}O$ is, respectively, ca. 1‰ and 0.3‰ lower at 7 Ma compared to present day (Shackleton & Hall, 1995). At Sites U1335, 573, 851, and U1338, bulk $\delta^{18}O$ is on average ca. 0.5‰ higher at 7 Ma compared to modern (Table S1 in Supporting Information S1; Reghellin et al., 2015, 2020; Shackleton & Hall, 1995). These observations are consistent with warmer than present day SST off the Equator in the eastern EEP and lower than present day SST off the Equator in the western EEP and along the Equator (Figure 7). SST meridional gradients were hence steeper during the BB and the upward motion on subsurface water was likely more intense compared to present day (Pisias et al., 1995; Shackleton & Hall, 1995).

Considering the stronger equatorial circulation affecting Site U1335 during the BB, we would also expect higher sedimentation rates compared to Site 852, to the east. This is not the case and, at Site U1335 between 5 and 7 Myr, LSR averages 8.4 m/Myr compared to 18.0 m/Myr at Site 852 and 12.2 m/Myr at Site 853 (Figure 6). Higher LSR at Site 853 compared to Site U1335 suggests that the lower LSR at Site U1335 reflects greater carbonate dissolution at >4.3 km water depth compared to the 600 m shallower (>3.7 km) water depth at Site 853, rather than to lower biological production compared to other off-Equator sites.

Site migration is not considered to be the cause of high bulk $\delta^{18}O$ and LSRs during the BB at Site U1335 because high bulk $\delta^{18}O$ and LSRs also characterize, during the BB, on-Equator Sites U1338, 851, and 573

(Figure 6). Records at the latter sites are less affected by site migration because they remained within the equatorial upwelling zone during the last 7 Myr. Hence, high bulk $\delta^{18}O$ and LSRs at Site U1335 primarily reflect cooler SST and increased biological production generated by enhanced equatorial circulation during the BB.

Apart from the generally high values, the bulk $\delta^{18}O$ record at Site U1335 displays five $\delta^{18}O$ minima centered at about 5.0 and 5.8 Myr (Figure 5; Table S1 in Supporting Information S1). One possible explanation for these is the presence of authigenic carbonates in sediments (Hesse & Schacht, 2011). The isotopic composition of such carbonate can vary from 0‰ to −25‰ for $\delta^{13}C$ and from −2‰ to −3‰ for $\delta^{18}O$, depending on the precipitation conditions in sediment pores and oxic to suboxic microbial organic matter oxidation. The $\delta^{18}O$ minima in BB sediments might reflect the presence of ^{18}O-depleted authigenic carbonate in the sediment, as they correspond to intervals of high MS (Pälike et al., 2010; Figure S4 in Supporting Information S1) and of darker sediment color (Figure 3). The absence of correlative low peaks in the bulk $\delta^{13}C$ record suggests that the carbon isotope composition of authigenic carbonate is close to that of biogenic carbonate.

5. Conclusions

Our data from Site U1335 represent the first set of bulk carbonate content and stable isotope records spanning the last 7 Myr at a resolution >20 kyr from an off-Equator site in the northwestern sector of the EEP. Site U1335 is positioned at a similar latitude, ca. 1,800 km to the west, and at a deeper water depth compared to Leg 138 off-Equator sites from which corresponding data have been published (Farrell et al., 1995; Pisias et al., 1995; Shackleton & Hall, 1995). Our initial questions (Ch. 1) can thus be addressed as follows:

1. Bulk $\delta^{18}O$ and $\delta^{13}C$ records display high-frequency variation at Site U1335 similarly to on-Equator Sites 573, 851, and U1338 (Reghellin et al., 2015, 2020; Shackleton & Hall, 1995). These variations are coupled to high-frequency changes in $CaCO_3$%, sediment color and physical properties, and result from changes in biogenic sediment production, mainly in the upper mixed layer, and sediment preservation
2. The bulk $\delta^{18}O$ at Site U1335 displays higher values during the BB than other bulk $\delta^{18}O$ records measured off the Equator. It is on average 0.5‰ higher than at Site 852, located at identical latitudes over the last 7 Myr. This observation indicates cooler SSTs generated by stronger equatorial upwelling to the west of the EEP, compared to the east
3. Sedimentation rates at Site U1335 are higher during BB times compared to post-BB times, but are lower compared to both on-Equator and off-Equator sites examined in the study. This implies both (a) enhanced biological production during BB times compared to post-BB times and (b) greater carbonate dissolution at Site U1335 compared to other sites, due to its several hundreds of meters greater water depth
4. The new bulk carbonate and stable isotope data from Site U1335 are consistent with a more intense wind-driven upwelling and expanded SST meridional gradients in the EEP during the BB (Pisias et al., 1995). The zonal SST gradient at ca. 5°N latitude during the BB seems to reflect more tilted isotherm contour patterns, with the equatorial circulation being less parallel to the Equator compared to present day

The results presented here represent only the starting point in the effort toward understanding the BB in the EEP. We are aware that the SST gradients inferred from bulk $\delta^{18}O$ are only in part consistent with SST reconstructions based on other proxies (e.g., Liu et al., 2019). A step toward further improving our understanding of how the BB manifests in the EEP would be to generate high resolution bulk $CaCO_3$% and stable isotopes records at multiple locations from an even wider area of the EEP (Figure 7). To quantify SST across the EEP bulk $\delta^{18}O$ and direct SST proxy records, such as $U^{k'}_{37}$ and TEX_{86}, need to be generated from the same location and at high temporal resolution. Certainly, bulk $\delta^{18}O$ data at Site U1335 reveal a more complicated spatial distribution of the BB than originally thought.

Data Availability Statement

Data generated in this study are available at https://doi.org/10.17043/reghellin-2022-sediment-1. Source of published data: Site 573: Mayer et al. (1985), Reghellin et al. (2015), and Weinreich and Theyer (1985). Site 851: Pisias et al. (1995), Raffi and Flores (1995), Reghellin et al. (2020), Shackleton and Hall (1995), and Shipboard Scientific Party (1992). Sites 852 and 853: Pisias et al. (1995), Raffi and Flores (1995), and Shackleton and

Hall (1995). Site U1335: Lyle et al. (2019) and Pälike et al. (2010). Site U1338: Backman et al. (2013), Pälike et al. (2010), and Reghellin et al. (2013, 2015)

Acknowledgments
We thank Klara Hajnal and Carina Johansson for sample preparations, Heike Siegmund for mass spectrometer analyses, Thomas Westerhold for providing the spliced core image, and Rebecca S. Robison for providing surface sediment samples. We also thank three anonymous reviewers for comments that improved the manuscript. We are grateful to the Integrated Ocean Discovery Program for providing the samples. This study was funded by Stockholm University and the Swedish Research Council (VR; Dnr 2010-3185). Open access funding provided by Universita degli Studi di Urbino Carlo Bo within the CRUI-CARE Agreement.

References

Anderson, T. F., & Steinmetz, J. C. (1981). Isotopic and biostratigraphical records of calcareous nannofossils in a Pleistocene core. *Nature*, *294*, 741–744. https://doi.org/10.1038/294741a0

Anderson, T. F., & Steinmetz, J. C. (1983). Stable isotopes in calcareous nannofossils: Potential application to deep-sea paleoenvironmental reconstructions during the Quaternary. *Utrecht Micropaleontological Bulletins*, *30*, 189–204.

Archer, D. E. (1991). Equatorial Pacific calcite preservation cycles: Production or dissolution? *Paleoceanography*, *6*, 561–571. https://doi.org/10.1029/91PA01630

Auer, G., De Vleeschouwer, D., Smith, R. A., Bogus, K., Groeneveld, J., Grunert, P., et al. (2019). Timing and pacing of Indonesian throughflow restriction and its connection to Late Pliocene climate shifts. *Paleoceanography and Paleoclimatology*, *34*, 635–657. https://doi.org/10.1029/2018PA003512

Backman, J., Raffi, I., Ciummelli, M., & Baldauf, J. (2013). Species-specific responses of late Miocene *Discoaster* spp. to enhanced biosilica productivity conditions in the equatorial Pacific and the Mediterranean. *Geo-Marine Letters*, *33*(4), 285–298.

Barber, R. T., & Chávez, F. P. (1986). Ocean variability in relation to living resources during the 1982–83 El Niño. *Nature*, *319*, 279–285. https://doi.org/10.1038/319279a0

Beltran, C., Rousselle, G., Backman, J., Wade, B. S., & Sicre, M.-A. (2014). Palaeoenvironmental conditions for the development of calcareous nannofossil acme during the late Miocene in the eastern equatorial Pacific. *Paleoceanography*, *29*, 210–222. https://doi.org/10.1002/2013PA002506

Berger, W. H. (1973). Deep-sea carbonates: Pleistocene dissolution cycles. *Journal of Foraminiferal Research*, *3*, 187–195.

Bolton, C. T., Gibbs, S. J., & Wilson, P. A. (2010). Evolution of nutricline dynamics in the equatorial Pacific during the late Pliocene. *Paleoceanography*, *25*, PA1207. https://doi.org/10.1029/2009PA001821

Brierley, C. M., & Fedorov, A. V. (2016). Comparing the impacts of Miocene-Pliocene changes in inter-ocean gateways on climate: Central American Seaway, Bering Strait, and Indonesia. *Earth and Planetary Science Letters*, *444*, 116–130. https://doi.org/10.1016/j.epsl.2016.03.010

Conan, S. M.-H., Ivanova, E. M., & Brummer, G.-J. A. (2002). Quantifying carbonate dissolution and calibration of foraminifera dissolution indices in the Samali Basin. *Marine Geology*, *182*, 325–349.

Conroy, J. L., Cobb, K. M., Lynch-Stieglitz, J., & Polissar, P. J. (2014). Constraints on the salinity-oxygen isotope relationship in the central tropical Pacific Ocean. *Marine Chemistry*, *161*, 26–33.

Dekens, P. S., Ravelo, A. C., & McCarthy, M. D. (2007). Warm upwelling regions in the Pliocene warm period. *Paleoceanography*, *22*, PA3211. https://doi.org/10.1029/2006PA001394

Dickens, G. R., & Owen, R. M. (1999). The latest Miocene-early Pliocene biogenic bloom: A revised Indian ocean perspective. *Marine Geology*, *161*, 75–91. https://doi.org/10.1016/S0025-3227(99)00057-2

Drury, A. J., Lee, G. P., Gray, W. R., Lyle, M., Westerhold, T., Shevenell, A. E., & John, C. M. (2018). Deciphering the state of the late Miocene to early Pliocene equatorial Pacific. *Paleoceanography and Paleoclimatology*, *33*. https://doi.org/10.1002/2017PA003245

Farrell, J. W., & Prell, W. L. (1989). Climatic change and $CaCO_3$ preservation: An 800,000 year bathymetric reconstruction from the central equatorial Pacific Ocean. *Paleoceanography*, *4*, 447–466. https://doi.org/10.1029/PA004i004p00447

Farrell, J. W., Raffi, I., Janecek, T. C., Murray, D. W., Levitan, M., Dadey, K. A., et al. (1995). Late Neogene sedimentation patterns in the eastern equatorial Pacific Ocean. In N. G.Pisias, L. A.Mayer, T. R.Janecek, A.Palmer-Julson, & T. H.van Andel (Eds.), *Proc. ODP, Sci. Results* (Vol. 138, pp. 717–756). College Station, TX: Ocean Drilling Program. https://doi.org/10.2973/odp.proc.sr.138.143.1995

Fiedler, P., & Lavín, F. M. (2017). Oceanographic conditions of the eastern tropical Pacific. In P. W. Glynn, D. Manzello, & I. Enochs (Eds.), *Coral Reefs of the eastern Tropical Pacific*. *Coral Reefs of the World 8*. https://doi.org/10.1007/978-94-017-7499-4_3

Ford, H. L., Ravelo, A. C., & Hovan, S. (2012). A deep eastern equatorial pacific thermocline during the early Pliocene warm period. *Earth and Planetary Science Letters*, *355*(356), 152–161. https://doi.org/10.1016/j.epsl.2012.08.027

Ford, H. L., Ravelo, A. C., & Polissar, P. J. (2015). *Reduced El Niño-Southern oscillation during the last glacial maximum*. Science, 347, 255–259. doi.org/10.1126/science.1258437

Garzione, C. N., Hoke, G. D., Libarkin, J. C., Withers, S., Macfadden, B. J., Eiler, J., et al. (2008). Rise of the Andes. *Science*, *320*, 1304–1307.

Grant, K. M., & Dickens, G. R. (2002). Coupled productivity and carbon isotope records in the southwest Pacific Ocean during the late Miocene-early Pliocene biogenic bloom. *Palaeogeography, Palaeoclimatology, Palaeoecology*, *187*, 61–82. https://doi.org/10.1016/S0031-0182(02)00508-4

Hagino, K., Okada, H., & Matsuoka, H. (2000). Spatial dynamics of coccolithophore assemblages in the equatorial western-central Pacific Ocean. *Marine Micropaleontology*, *39*, 53–72. https://doi.org/10.1016/S0377-8398(00)00014-1

Hayward, B. W., Neil, H., Carter, R., Grenfell, H. R., & Hayward, J. J. (2002). Factors influencing the distribution patterns of recent deep-sea benthic foraminifera, east of New Zealand, Southwest Pacific Ocean. *Marine Micropaleontology*, *46*(1), 139–176.

Hesse, R., & Schacht, U. (2011). Early diagenesis of deep-sea sediments. *Developments in Sedimentology*, *63*, 557–713. https://doi.org/10.1016/B978-0-444-53000-4.00009-3

Holbrook, N. J., Brown, J. N., Davidson, J., Feng, M., Hobday, A. J., Lough, J. M., et al. (2012). El Niño-Southern oscillation. In E. S.Poloczanska, A. J.Hobday, & A. J.Richardson (Eds.), *A marine climate change impacts and adaptation report card for Australia 2012*.

Honjo, S., Dymond, J., Collier, R., & Manganini, S. J. (1995). Export production of particles to the interior of the equatorial Pacific Ocean during the 1992 EqPac experiment. *Deep Sea Research Part II: Topical Studies in Oceanography*, *42*, 831–870.

Honjo, S., & Okada, H. (1974). Community structure of coccolithophores in the photic layer of the mid-Pacific. *Micropaleontology*, *20*, 209–230.

Hovan, S. A. (1995). Late Cenozoic atmospheric circulation intensity and climatic history recorded by eolian deposition in the eastern equatorial Pacific Ocean, Leg 138. In N. G.Pisias, L. A.Mayer, T. R.Janecek, A.Palmer-Julson, & T. H.van Andel (Eds.), *Proc. ODP, Sci. Results* (Vol. 138, pp. 615–625). College Station, TX: Ocean Drilling Program. https://doi.org/10.2973/odp.proc.sr.138.132.1995

Kessler, W. S. (2006). The circulation of the eastern tropical Pacific: A review. *Progress in Oceanography*, *69*, 181–217. https://doi.org/10.1016/j.pocean.2006.03.009

Kosaka, Y., & Xie, S. P. (2013). Recent global-warming hiatus tied to equatorial Pacific surface cooling. *Nature*, *501*, 403–407. https://doi.org/10.1038/nature12534

Kozyr, A. (2008). *Global ocean surface water partial pressure of CO_2 database: Measurements performed during 1968-2007 (version 2007)*. Oak Ridge, TN: Oak Ridge National Laboratory (ORNL).

Kroopnick, P. M. (1985). The distribution of ^{13}C of ΣCO_2 in the world oceans. *Deep Sea Research Part A, Oceanographic Research Papers*, *32*, 57–84. https://doi.org/10.1016/0198-0149(85)90017-2

Lariviere, J. P., Ravelo, A. C., Crimmins, A., Dekens, P. S., Ford, H. L., Lyle, M. W., & Wara, M. W. (2012). Late Miocene decoupling of oceanic warmth and atmospheric carbon dioxide forcing. *Nature*, *486*, 97–100. https://doi.org/10.1038/nature11200

Lawrence, K. T., Liu, Z., & Herbert, T. D. (2006). Evolution of the eastern tropical Pacific through Plio-Pleistocene glaciation. *Science*, *312*, 79–83. https://doi.org/10.1126/science.1120395

Lea, D. W. (2014). Not so permanent El Ninõ. *Science*, *344*, 52–53. https://doi.org/10.1126/science.1252246

Linsley, B. K., Wu, H. C., Dassié, E. P., & Schrag, D. P. (2015). Decadal changes in South Pacific sea surface temperatures and the relationship to the Pacific decadal oscillation and upper ocean heat content. *Geophysical Research Letters*, *42*, 2358–2366. https://doi.org/10.1002/2015GL063045

Liu, J., Tian, J., Liu, Z., Herbert, T. D., Fedorov, A. V., & Lyle, M. W. (2019). Eastern equatorial Pacific cold tongue evolution since the late Miocene linked to extratropical climate. *Science Advances*, *5*(4), eaau6060.

Locarnini, R. A., Mishonov, A. V., Baranova, O. K., Boyer, T. P., Zweng, M. M., Garcia, H. E., et al. (2019). World Ocean Atlas 2018In In A.Mishonov Technical (Ed.), *Volume 1: Temperature. NOAA Atlas NESDIS 81*.

Lourens, L. J., Hilgen, F. J., Shackleton, N. J., Laskar, J., & Wilson, D. (2004). The Neogene period. In F. M.Gradstein, J. G.Ogg, & A. G.Smith (Eds.), *A geological time scale 2004* (pp. 409–440). Cambridge, UK: Cambridge University Press.

Lyle, M. (2003). Neogene carbonate burial in the Pacific Ocean, *Paleoceanography*, *18*(3), 1059. https://doi.org/10.1029/2002PA000777

Lyle, M., Dadey, K. A., & Farrell, J. W. (1995). The late Miocene (11–8 Ma) eastern Pacific carbonate crash: Evidence for reorganization of deep-water circulation by the closure of the Panama Gateway. In N. G.Pisias, L. A.Mayer, T. R.Janecek, A.Palmer-Julson, & T. H.van Andel (Eds.), *Proc. ODP, Sci. Results* (Vol. 138, pp. 821–838). College Station, TX: Ocean Drilling Program. https://doi.org/10.2973/odp.proc.sr.138.157.1995

Lyle, M. W., & Baldauf, J. (2015). Biogenic sediment regimes in the Neogene equatorial Pacific, IODP Site U1338: Burial, production, and diatom community. *Palaeogeography, Palaeoclimatology, Palaeoecology*, *433*, 106–128. https://doi.org/10.1016/j.palaeo.2015.04.001

Lyle, M. W., Drury, A. J., Tian, J., Wilkens, R., & Westerhold, T. (2019). Late Miocene to Holocene high-resolution eastern equatorial pacific carbonate records: Stratigraphy linked by dissolution and paleoproductivity. Climate of the Past, *15*, 1715–1739. https://doi.org/10.5194/cp-15-1715-2019

Lyle, M. W., & Wilson, P. A. (2006). Leg 199 synthesis: Evolution of the equatorial Pacific in the early Cenozoic. In P. A.Wilson, M.Lyle, & J. V.Firth (Eds.), Proc. ODP, Sci. Results (Vol. 199, pp. 1–39). College Station, TX: Ocean Drilling Program. https://doi.org/10.2973/odp.proc.sr.199.201.2006

Mayer, L., Theyer, F., Barron, J. A., Dunn, D. A., Handyside, T., Hills, S., & Shipboard Scientific Party. (1985). Site 573. In L.Mayer, F. Theyer, J. A. Barron, D. A. Dunn, T. Handyside, S. Hills, et al. (Eds.), *Proceedings of the Deep Sea Drilling Project, Init. Rep* (Vol. 85, pp. 137–223). Washington, DC: Deep Sea Drilling Project.

Mörth, C.-M., & Backman, J. (2011). Practical steps for improved estimates of calcium carbonate concentrations in deep sea sediments using coulometry. *Limnology and Oceanography: Methods*, *9*, 565–570. https://doi.org/10.4319/lom.2011.9.565

Nathan, S. A., & Leckie, R. M. (2009). Early history of the Western Pacific Warm Pool during the middle to late Miocene (~ 13.2–5.8 Ma): Role of sea-level change and implications for equatorial circulation. *Palaeogeography, Palaeoclimatology, Palaeoecology*, *274*(3-4), 140–159.

O'Dea, A., Lessios, H. A., Coates, A. G., Eytan, R. I., Restrepo-Moreno, S. A., Cione, A. L., et al. (2016). Formation of the Isthmus of Panama. *Science Advances*, *2*(8), e1600883.

Pälike, H., Lyle, M. W., Nishi, H., Raffi, I., Ridgwell, A., Gamage, K., et al. (2012). A Cenozoic record of the equatorial Pacific carbonate compensation depth. *Nature*, *488*, 609–614. https://doi.org/10.1038/nature11360

Pälike, H., Nishi, H., Lyle, M. W., Raffi, I., Gamage, K., Klaus, A., & Shipboard Scientists. (2010). Expedition 320/321 summary. In H.Pälike, M.Lyle, H.Nishi, I.Raffi, K.Gamage, A.Klaus (Eds.), & the Expedition 320/321 Scientists. (Eds.), *Proc. IODP* (Vol. 320/321). Tokyo: Integrated Ocean Drilling Program Management International, Inc. https://doi.org/10.2204/iodp.proc.320321.101.2010

Pennington, J. T., Mahoney, K. L., Kuwahara, V. S., Kolber, D. D., Calienes, R., & Chavez, F. P. (2006). Primary production in the eastern tropical Pacific: A review. *Progress in Oceanography*, *69*, 285–317. https://doi.org/10.1016/j.pocean.2006.03.012

Peterson, L. C., & Backman, J. (1990). Late Cenozoic carbonate accumulation and the history of the carbonate compensation depth in the western equatorial Indian Ocean. In R. A.Duncan, J.Backman, L. C.Peterson, P. A. Baker, A. N. Baxter, A. Boersma, et al. (Eds.), *Proc. ODP, Sci. Results* (Vol. 115, pp. 467–507). College Station, TX: Ocean Drilling Program. https://doi.org/10.2973/odp.proc.sr.115.163.1990

Pisias, N. G., Mayer, L. A., & Mix, A. C. (1995). Paleoceanography of the eastern equatorial Pacific during the Neogene: Synthesis of Leg 138 drilling results. In N. G.Pisias, L. A.Mayer, T. R.Janecek, A.Palmer-Julson, & T. H.van Andel (Eds.), *Proc. ODP, Sci. Results* (Vol. 138, pp. 5–21). College Station, TX: Ocean Drilling Program. https://doi.org/10.2973/odp.proc.sr.138.101.1995

Pisias, N. G., & Prell, W. L. (1985). Changes in calcium carbonate accumulation in the equatorial Pacific during the late Cenozoic: Evidence from HPC Site 572. In *The carbon cycle and atmospheric CO2: Natural variations Archean to present* (Vol. *32*, pp. 443–454). Washington, DC: AGU.

Raffi, I., & Flores, J.-A. (1995). Pleistocene through Miocene calcareous nannofossils from eastern equatorial Pacific Ocean (Leg 138). In N. G.Pisias, L. A.Mayer, T. R.Janecek, A.Palmer-Julson, & T. H.van Andel (Eds.), *Proc. ODP, Sci. Results* (Vol. 138, pp. 233–286). College Station, TX: Ocean Drilling Program. https://doi.org/10.2973/odp.proc.sr.138.112.1995

Ravelo, A. C. (2010). Palaeoclimate: Warmth and glaciation. *Nature Geoscience*, *3*, 672–674. https://doi.org/10.1038/ngeo965

Ravelo, A. C., Dekens, P. S., & McCarthy, M. D. (2006). Evidence for El Niño-like conditions during the Pliocene. *Geological Society of America Today*, *16*, 4–11. https://doi.org/10.1130/1052-5173(2006)016<4

Reghellin, D., Coxall, H. K., Dickens, G. R., & Backman, J. (2015). Carbon and oxygen isotopes of bulk carbonate in sediment deposited beneath the eastern equatorial Pacific over the last 8 million years. *Paleoceanography*, *30*, 1261–1286. https://doi.org/10.1002/2015PA002825

Reghellin, D., Dickens, G. R., & Backman, J. (2013). The relationship between wet bulk density and carbonate content in sediments from the Eastern Equatorial Pacific. *Marine Geology*, *344*, 41–52. https://doi.org/10.1016/j.margeo.2013.07.007

Reghellin, D., Dickens, G. R., Coxall, H. K., & Backman, J. (2020). Understanding bulk sediment stable isotope records in the Eastern Equatorial Pacific, from seven million years ago to present day. *Paleoceanography and Paleoclimatology*, *35*, e2019PA003586. https://doi.org/10.1029/2019PA003586

Révész, K. M., & Landwehr, J. M. (2002). δ13C and δ18O isotopic composition of CaCO3 measured by continuous flow isotope ratio mass spectrometry: Statistical evaluation and verification by application to Devils hole core DH-11 calcite. *Rapid Communications in Mass Spectrometry*, *16*, 2102–2114.

Rousselle, G., Beltran, C., Sicre, M. A., Raffi, I., & De Rafélis, M. (2013). Changes in sea-surface conditions in the Equatorial Pacific during the middle Miocene-Pliocene as inferred from coccolith geochemistry. *Earth and Planetary Science Letters*, *361*, 412–421. https://doi.org/10.1016/j.epsl.2012.11.003

Schneider, N. (1998). The Indonesian throughflow and the global climate system. *Journal of Climate*, *11*, 676–689.

Seki, O., Schmidt, D. N., Schouten, S., Hopmans, E. C., Sinninghe Damsté, J. S., & Pancost, R. D. (2012). Paleoceanographic changes in the eastern equatorial Pacific over the last 10 Myr. *Paleoceanography*, *27*, PA3224. https://doi.org/10.1029/2011PA002158

Shackford, J. K., Lyle, M., Wilkens, R., & Tian, J. (2014). Data report: Raw and normalized elemental data along the site U1335, U1336, and U1337 splices from X-ray fluorescence scanning. In H.Pälike, M.Lyle, H.Nishi, I.Raffi, K.Gamage, A.Klaus (Eds.), & The Expedition 320/321 Scientists (Eds.), *Proc. IODP* (Vol. 320/321). Tokyo: Integrated Ocean Drilling Program Management International, Inc. https://doi.org/10.2204/iodp.proc.320321.216.2014

Shackleton, N. J., & Hall, M. A. (1995). Stable isotope records in bulk sediments (Leg 138). In N. G.Pisias, L. A.Mayer, T. R.Janecek, A.Palmer-Julson, & T. H.van Andel (Eds.), *Proc. ODP, Sci. Results* (Vol. 138, pp. 797–805). College Station, TX: Ocean Drilling Program. https://doi.org/10.2973/odp.proc.sr.138.150.1995

Shipboard Scientific Party. (1992). Site 851. In L.Mayer, N.Pisias, T. R.Janecek, J. G. Baldauf, S. F. Bloomer, K. A. Dadey, et al. (Eds.), *Proc. ODP, Init. Rep* (Vol. 138, pp. 891–965). College Station, TX: Ocean Drilling Program. https://doi.org/10.2973/odp.proc.ir.138.116.1992

Steinmetz, J. C. (1994). Stable isotopes in modern coccolithophoresIn In A.Winter, & W. G.Siesser (Eds.), *Coccolithophores* (pp. 219–229). Cambridge, UK: Cambridge University Press.

Steinthorsdottir, M., Coxall, H. K., De Boer, A. M., Huber, M., Barbolini, N., Bradshaw, C. D., et al. (2021). The Miocene: The future of the past. *Paleoceanography and Paleoclimatology*, *36*, e2020PA004037. https://doi.org/10.1029/2020PA004037

Steph, S., Tiedemann, R., Prange, M., Groeneveld, J., Schulz, M., Timmermann, A., et al. (2010). Early Pliocene increase in thermohaline overturning: A precondition for the development of the modern equatorial Pacific cold tongue. *Paleoceanography*, *25*, PA2202. https://doi.org/10.1029/2008PA001645

Tagliabue, A., & Bopp, L. (2008). Towards understanding global variability in ocean carbon-13. *Global Biogeochemical Cycles*, *22*, GB1025. https://doi.org/10.1029/2007GB003037

Takahashi, T., Sutherland, S. C., Sweeney, C., Poisson, A., Metzl, N., Tilbrook, B., et al. (2002). Global sea-air CO_2 flux based on climatological surface ocean pCO_2, and seasonal biological and temperature effects. *Deep Sea Research Part II: Topical Studies in Oceanography*, *49*, 1601–1622. https://doi.org/10.1016/S0967-0645(02)00003-6

Takahashi, T., Sutherland, S. C., Wanninkhof, R., Sweeney, C., Feely, R. A., Chipman, D. W., et al. (2009). Climatological mean and decadal change in surface ocean pCO_2, and net sea-air CO_2 flux over the global oceans. *Deep Sea Research Part II: Topical Studies in Oceanography*, *56*, 554–577. https://doi.org/10.1016/j.dsr2.2008.12.009

Trenberth, K., & Caron, J. (2000). The southern oscillation revisited: Sea level pressures, surface temperatures, and precipitation. *Journal of Climate*, *13*, 4358–4365.

van Andel, T. H., Heath, G. R., & Moore, T. C. (1975). *Cenozoic history and paleoceanography of the Central Equatorial Pacific Ocean: A regional synthesis of Deep Sea Drilling Project Data* (Vol. 143). Geological Society of America. https://doi.org/10.1175/1520-0442(2000)013<4358:TSORSL>2.0.CO;2

Wara, M. W., Ravelo, A. C., & Delaney, M. L. (2005). Climate change: Permanent El Niño-like conditions during the Pliocene warm period. *Science*, *309*, 758–761. https://doi.org/10.1126/science.1112596

Weinreich, N., & Theyer, F. (1985). Paleomagnetism of Deep Sea Drilling Project Leg 85 sediments: Neogene magnetostratigraphy and tectonic history of the central equatorial Pacific. In L.Mayer, F. Theyer, J. A. Barron, D. A. Dunn, T. Handyside, S. Hills, et al. (Eds.), *Proceedings of the Deep Sea Drilling Project*, Init. Rep. (Vol. 85, pp. 849–901). Washington, DC: Deep Sea Drilling Project. https://doi.org/10.2973/dsdp.proc.85.129.1985

Zhang, Y. G., Pagani, M., Henderiks, J., & Ren, H. (2017). A long history of equatorial deep-water upwelling in the Pacific Ocean. *Earth and Planetary Science Letters*, *467*, 1–9. https://doi.org/10.1016/j.epsl.2017.03.016

Zhang, Y. G., Pagani, M., & Liu, Z. (2014). A 12-million-year temperature history of the tropical Pacific Ocean. *Science*, *344*(6179), 84–87.